Directed Evolution of Excited State Lifetime and Brightness in FusionRed using a Microfluidic Sorter

Journal:	*Integrative Biology*
Manuscript ID	IB-ART-06-2018-000103.R1
Article Type:	Paper
Date Submitted by the Author:	19-Jul-2018

Complete List of Authors:	Manna, Premashis; University of Colorado Boulder, Chemistry and Biochemistry; University of Colorado Boulder, JILA Hung, Sheng-Ting; University of Colorado, JILA Mukherjee, Srijit; University of Colorado, JILA; University of Colorado, Department of Chemistry and Biochemistry Friis, Pia; University of Colorado, JILA Simpson, David; University of Colorado Boulder, Chemistry and Biochemistry Hindt, Maria; University of Colorado, Department of Chemistry and Biochemistry Palmer, Amy; University of Colorado Boulder, Chemistry and Biochemistry Jimenez, Ralph; University of Colorado, JILA and Department of Chemistry and Biochemistry; National Institutes of Standards and Technology,

Red Fluorescent Proteins (RFPs) are advantageous for live-cell imaging owing to the low optical attenuation and phototoxicity for excitation beyond 550 nm. FusionRed, an RFP optimized for high fusion efficiency, low dimerization *in vivo* and low cytotoxicity in cells and tissues, is dim compared to more widely-used RFPs. We developed a microfluidic flow cytometer for sorting cell-based libraries employing both fluorescence lifetime and brightness criteria and use it to (1) visualize photophysical evolution of the clones, (2) increase the fluorescence quantum yield leading to improved brightness in FusionRed variants expressed in yeast cells, and (3) produce a two-fold improvement in brightness of a FusionRed variant expressed in mammalian cells, making it comparable to that of mCherry, the most widely-used RFP.

Directed Evolution of Excited State Lifetime and Brightness in FusionRed using a Microfluidic Sorter

Premashis Manna[1], *Sheng-Ting Hung*[1], *Srijit Mukherjee*[1,2], Pia *Friis*[1], *David M. Simpson*[3], *Maria Lo*[3], *Amy E. Palmer*[2,3], *Ralph Jimenez*[1,2]

[1]JILA, NIST, and University of Colorado, Boulder, Colorado 80309, United States
[2]Department of Chemistry and Biochemistry, University of Colorado, Boulder, Colorado 80309, United States
[3]BioFrontiers Institute, University of Colorado, Boulder, Colorado 80309, United States

ABSTRACT

Green fluorescent proteins (GFP) and their blue, cyan and red counterparts offer unprecedented advantages as biological markers owing to their genetic encodability and straightforward expression in different organisms. Although significant advancements have been made towards engineering key photo-physical properties of red fluorescent proteins (RFPs), they continue to perform sub-optimally relative to GFP variants. Advanced engineering strategies are needed for further evolution of RFPs in the pursuit of improving their photo-physics. In this report, a microfluidic sorter that discriminates members of a cell-based library based on their excited state lifetime and fluorescence intensity is used for the directed evolution of the photo-physical properties of FusionRed. In-flow measurements of the fluorescence lifetime are performed in a frequency-domain approach with sub-millisecond sampling times. Promising clones are sorted by optical force trapping with an infrared laser. Using this microfluidic sorter, mutants are generated with longer lifetimes than their precursor, FusionRed. This improvement in excited state lifetime of the mutants leads to an increase in their fluorescence quantum yield up to 1.8-fold. In the course of evolution, we also identified one key mutation (L177M), which generated a mutant (FusionRed-M) that displayed ~2-fold higher brightness than its precursor upon expression in mammalian (HeLa) cells. Photo-physical and mutational analyses of clones isolated at the different stages of mutagenesis, reveals the photo-physical evolution towards higher *in vivo* brightness.

INTRODUCTION

Fluorescent proteins (FPs) have become an indispensable tool for biological and biomedical research because their genetic encodability makes them exceptional probes for tracking cellular components in specific cellular compartments[1]. The red fluorescent proteins are excited with relatively long wavelengths of visible light beyond the absorption bands of endogenous cellular constituents, so they are particularly useful for imaging of tissues and long-term imaging with minimal photo-toxicity[2]. This utility motivates the engineering of brighter, more photostable FPs with red-shifted emission[3-6].

The main drawback of RFPs is their lower brightness compared to the green and yellow FPs. The cellular brightness for time-lapse imaging of FPs depends on many factors including the extinction coefficient, fluorescence quantum yield, expression levels (controlled by chromophore maturation, protein folding and expression from the DNA to the protein level) and photostability. Most widely-used FPs have been developed by engineering the chromophore-forming residues, their immediate environment[7, 8] or dimeric interfaces[9] combined with random mutagenesis. Several rounds of mutagenesis and selection are usually required to obtain an FP with improved properties. There is evidence that mutations in the distal regions of the β-barrel can modulate the photo-physical properties of the FPs in unique ways, *e.g.* through fluctuations of the β-barrel[10, 11]. Engineering of these residues could enhance the photo-physical diversity of the library designs and facilitate the development of substantially improved, next-generation FPs. However, the effects of individual mutations are often context-dependent and co-evolve with other residues but inclusion of additional target residues increases the library size exponentially[12]. These considerations drive the need for high information-content, high-throughput cell selection methods. Conventional methods include screening on plates[8], and/or fluorescence-activated cell sorting (FACS). Methods for screening of bacterial colonies is moving towards higher information content. For example, Mizuno and coworkers used an automated imaging system to develop photoswitchable variants of Dronpa[13], and Duwe et al. screened ~10^5 colonies to isolate photoswitchable versions of enhanced GFP[14]. Also, a fluorescence lifetime imaging system was utilized to acquire a fluorescence lifetime image of an entire petri dish to determine the lifetime and brightness of individual bacterial colonies[15]. Since the fluorescence quantum yield of FPs is correlated to the fluorescence lifetime (SI-Fig. S1), FPs with high quantum yield and brightness can be selected[11, 15, 16]. A limitation of plate-based screening is that measurements on colonies average over many cells, leaving unresolved heterogeneity of photo-physical and biochemical properties at the single-cell level. This heterogeneity can be significant and critical for applications of FPs and biosensors based on them[17, 18]. As an example, Arnfinnsdottir et. al.'s work on heterogeneity in GFP expression in isogenic populations of *P. putida* elucidated how the clonal populations do not always scale to individual cellular behavior[18]. Such heterogeneities are avoided when one uses single cell FACS based methods to characterize photo-physical properties in cells.

In contrast, FACS is capable of screening >10^7 member libraries with high throughput at single cell resolution. Wang et al. employed multiple rounds of FACS-based sorting of FP libraries to generate mPlum by red-shifting the emission wavelength of a DsRed variant[19]. However, FACS-based selections are limited to fluorescence intensity at a few excitation/emission wavelengths. To explore the broad fitness landscape of FPs and select mutants with a diverse range of photo-physical properties, more sophisticated fluorescence-based cell sorting techniques are required. For example, fluorescence lifetime is directly proportional to the quantum yield and independent of expression level. Hence, increasing fluorescence lifetime directly leads to enhancement of quantum yield (SI-Sec. 1), and thus improved brightness if there is no or little change in extinction coefficient. Both time and frequency-domain fluorescence lifetime measurements have been implemented into flow cytometry but the application in directing the evolution of FP libraries towards higher quantum yield has not yet been described.

Frequency-domain lifetime methods utilize sinusoidal modulation of the excitation laser at radio frequencies, resulting in fluorescence signals oscillating at the same frequency (ω) as the excitation but with a phase shift (θ) that is related to the excited state lifetime (τ) of the fluorophore:

$$\theta = tan^{-1}(\omega\tau).$$

Therefore, the measurement of phase shift reveals the excited state lifetime of the fluorophore (SI-Sec. 6). Although time-domain approaches are capable of extracting the multi-exponential nature of fluorescence decay in a flow cytometric platform[20], we use a frequency-domain technique due to its relatively higher throughput and simplicity of implementation with a commercial high-speed lock-in amplifier.

Frequency-domain flow cytometry was first demonstrated to measure fluorescence lifetimes from fluorescent beads and cells labeled with dyes, which exhibit similar emission spectra that are difficult to resolve[21, 22]. Though fluorescence lifetime measurement combined with flow cytometry was mostly used for the purpose of analysis and screening in early developments[23, 24], many recent efforts have been made to incorporate sorting ability. Cao et al. used the analog method[22] to sort cells and beads labeled with fluorophores with spectrally overlapping fluorescence based on the lifetime, with *a priori* knowledge of the fluorophore lifetimes[25].This approach utilizes an intensity-modulated excitation source and requires phase sensitive detection electronics to obtain the average fluorescence lifetime. Houston and coworkers demonstrated sorting fluorescent beads based on digitally modulated excitation source and lifetime analysis using the frequency-domain technique modified with an open reconfigurable cytometric acquisition system capable of digital signal-processing[26]. Though *a priori* knowledge of the lifetimes of the fluorophores is not required in the digital system, the system loses out to the better signal to noise ratios seen in analog systems. Using the digital system, Sands et al. developed a method to simultaneously measure the phase delay related to the fluorescence lifetime and the emission modulation depth as an additional criterion, and demonstrated the ability to sort cells expressing isospectral FPs with differing lifetimes[27]. The digital technique was further developed by Yang et al. to screen two near-infrared FPs based on lifetimes, demonstrating the ability to distinguish two FPs with similar emission intensity[28]. While these studies demonstrated sorting cells containing a small set (usually two kinds) of FPs based on the fluorescence lifetime, there is no report on sorting an FP library and its applications.

We first reported a microfluidic platform capable of selecting RFP mutants with improved photostability[29, 30]. In another study, multiparameter photo-physical analysis of RFP libraries was performed to quantify the brightness, photostability and fluorescence lifetime of cell-based libraries using a custom-built analog phase sensitive microfluidic cytometry[31]. Here, we describe further development in combining sorting with lifetime measurements on libraries of FusionRed (abbreviated as FR), a protein developed to address the dimerization and cytotoxicity issues observed in several RFPs[9]. With its reduced dimerization tendency[32], improved fusion efficiency and low cytotoxicity[9], FusionRed has the potential to be an excellent bio-marker for live-cell imaging, but its relatively low molecular brightness due to low fluorescence quantum yield and low cellular brightness relative to mCherry, the most commonly used RFP, limit its attractiveness. We hypothesized that an improvement in excited state lifetime would lead to an increase in quantum yield of this FP, resulting in enhanced molecular brightness. We also hypothesized that the low

147 brightness of FusionRed in cells originates from low protein expression level since
148 the molecular brightness of FusionRed[9] is higher than mCherry[7]. We demonstrate
149 the use of our instrument to "watch" FusionRed clones evolving towards higher
150 quantum yield through multiple rounds of error-prone PCR (EP-PCR) mutagenesis
151 and selection. This process led to the generation of substantially brighter FusionRed
152 variants. To the best of our knowledge, our work is the first to report the use of a
153 frequency-domain flow cytometer for the directed evolution of FP lifetime, quantum
154 yield and brightness.
155
156 **EXPERIMENTAL SECTION**
157
158 **Microfluidic Design & Manifold Assembly**
159
160 We adopted a 2D hydrodynamic focusing microfluidic design from our previous work,
161 consisting of three inlets (sheath, sample and sheath) and two outlets (collection and
162 waste)[29, 33]. Cell suspensions are flowed through the middle channel, which is
163 focused to a narrow stream by two sheath channels. Details of the design are given
164 in SI-Fig. S2a. The chip is sealed to a polytetrafluoroethylene (PTFE) manifold with
165 O-rings (SI-Fig. S2b). Three inlets of the manifold are connected with and regulated
166 by three pressure-controllers (Pneutronics, OEM, EPS10-5-0-2) for independent
167 control of the flow in each channel. The inlet reservoirs of the manifold can be filled
168 with up to 150 µl of sample or sheath buffers. The two outlets (collection and waste)
169 are open to ambient pressure.
170
171 **Optical Set-up**
172
173 The optical set-up for the microfluidic sorter is presented in SI-Fig. S3. A 561-nm
174 laser (Genesis MX, Coherent, 1W) laser beam is split with a 70:30 beam splitter. The
175 higher power beam is directed through an electro-optic modulator (EOM, ThorLabs,
176 EO-AM-NR-C4) that amplitude-modulates the beam at a frequency of 29.5 MHz.
177 Before the beam enters the EOM, it is focused with a lens to fit into the EOM
178 aperture. Two polarizers (Newport) and a half-wave plate (Newport) are used to
179 control the power of the lifetime beam after the EOM. The lower power beam and the
180 modulated beam pass through a 150 mm plano-convex cylindrical lens, transforming
181 the circular beams into elliptical ones. The elliptical beams from the cylindrical lens
182 enter the side-port of a commercial inverted microscope (Olympus IX71), reflected
183 through a dichroic mirror (Semrock, FF573-Di01-25x36), and focused into the
184 microfluidic chip through an air-objective (Olympus, 20x, NA 0.45). The FWHM of the
185 lifetime beam is measured to be 9 µm and 56 µm in the minor and major axes of its
186 elliptical spatial mode, respectively. The other beam has similar dimensions.
187 Epifluorescence from cells expressing RFPs is separated from the excitation beams
188 using a band-pass filter (Semrock, FF01-629/56-25). Subsequently, the lifetime and
189 timing beams are spatially separated with mirrors and slits and collected by two red-
190 wavelength sensitive photo-multiplier tubes (PMT, Hamamatsu R9880U-20) as
191 illustrated in SI-Fig. S3.
192
193 **Detection Electronics**

194 The electronic components for detection, amplification and processing of
195 fluorescence signals are schematically illustrated in SI-Fig. S4. A function generator

(Agilent, 33520B) is used to provide a sinusoidally modulated electrical signal with 10 V (peak-to-peak) at 29.5 MHz to drive the EOM, and also send a 1 V peak-to-peak reference signal to the lock-in amplifier. The fluorescence signal obtained from the lifetime PMT is split into two components (high and low frequencies) using a biased-tee. The high frequency component (~ 30 MHz) is directed to a custom-made amplifier and then sent to a lock-in amplifier (Zurich Instruments, UHF) for frequency-domain lifetime measurements. The lock-in amplifier outputs in-phase and quadrature phase signals that are used for frequency-domain measurements of the excited state lifetime of the RFP mutants. The low frequency components (< 83 kHz) from the biased-tee, along with the signal from timing beam are further amplified with a home-built trans-impedance amplifier for improving the signal-to-noise ratios. Electronic amplification of the fluorescence signal from lifetime beam is achieved by either a linear or logarithmic trans-impedance amplifier. The logarithmic amplifier has higher dynamic range and thus helps to resolve the brightness of a mixture of mutants better than the linear amplifier (SI-Fig. S5). Finally, all the signals are digitized at 125 kHz, 16-bit resolution by a data acquisition card (DAQ, National Instruments BNC-209a, PCI-6251 with NI-SCX). The DAQ board communicates with a target computer that runs the LabView RealTime module to analyze the digitized data streams, identify the isolated non-overlapping bursts of peaks due to the passage of cells through the laser beams, and perform selection decisions based on user-defined thresholds of lifetime, fluorescence intensity or transit time of the cells. The Target computer is connected to a Host computer that controls the operation of the sorter and used for real-time data display.

Cell Culture, Library Generation, and Sample Preparation

We employ yeast (*Saccharomyces cerevisiae*) as the host organism for this work because we aimed to carry out a selection in eukaryotic cells rather than prokaryotic cells. Yeast also offer advantages in the library generation, screening, sorting because the recovery of yeast cells after sorting is faster than mammalian cells due to their fast doubling time (~90 minutes in yeast versus ~ 20 hrs in HeLa cells, respectively). However, the results suggest that RFPs developed from yeast cells do not necessarily retain their performance in mammalian cells, despite both being eukaryotic cells.

For all the EP-PCR libraries described in this report, a typical error-rate is used that incorporates ~5 mutations (at the nucleotide level) per template. To achieve this mutation rate, 100-500 ng of initial target DNA and 30 PCR cycles are used. Typical size of the EP-PCR library is ~ $3x10^6$. Assuming the mean mutation frequency per gene as 5 and length of template as 708 base pairs, each library contains ~ $2x10^6$ number of distinct full-length FP variants. The analysis of distinct mutants in EP-PCR libraries is based on the algorithm by Patrick et al[34]. Details of the library generation protocol are provided in SI-Sec. 7.

For the microfluidic screening of yeast cells containing RFPs, the corresponding library or the culture is freshly grown from a stored stock and expressed transiently. A 0.5 ml volume of stored culture media is added to 10 mL solution of growth media (yeast nitrogen base, ammonium sulphate, dextrose) and grown for 8 hrs. Next, 0.5 ml of this freshly-grown cell culture is added to 10 mL solution of induction media

(yeast nitrogen base, ammonium sulphate, galactose, raffinose). Cells are screened or sorted 17-20 hrs. after induction. During growth and expression, the cultures are incubated at 30°C and constantly shaken at 250 rpm.

For screening/sorting, yeast cells expressing the library are diluted (10-20 fold) with the blank media (yeast nitrogen base, ammonium sulphate) containing 14% OptiPrep (60% weight/volume iodixanol in water), and subsequently filtered using a 40 μm filter to remove cell debris prior to loading into the microfluidic chip.

Multi-parametric Screening

Microfluidic screening reveals the fluorescence intensity and excited state lifetime profiles of the individual mutants or RFP libraries (Figure 2a & b). Based on the initial screening results of a library, a decision is made to sort a sub-population of the library having significantly longer lifetime or/and higher fluorescence intensity for further enrichment and selection as described in greater detail in the Results section.

As a cell passes through lifetime and timing beams (Figure 1), fluorescence signals are detected by two PMTs. After signal processing (SI-Fig. S4), digitized data from the PMTs are analyzed by custom-made LabView software that quantifies the excited state lifetime of the mutants from the in-phase (V_I) and quadrature phase (V_Q) values provided by the lock-in amplifier (SI-Sec. 6).

For assessing the brightness of the mutants, the fluorescence intensity from the lifetime beam was used. During the microfluidic screening, either a linear or logarithmic amplifier was used for the amplification of lifetime PMT signal. Although, both amplifiers clearly resolve the excited state lifetime of the mutants, owing to its higher dynamic range, only the logarithmic amplifier captures the peak of the fluorescence intensity (SI-Fig. S5). The screening in the microfluidic setup is operated at a typical rate of ~30 cells/s, which optimizes the flow rates, signal processing and data storage in the current electronic and software configuration. Higher screening speeds can be achieved with faster electronics such as a field-programmable gate array (FPGA) based system.

Selection of Improved Fluorescent Protein Variants

Once the lifetime and brightness profiles of a RFP library are revealed through the microfluidic screening, the next step is to sort the mutants with desired photo-physical properties. We employ optical force gradient-based sorting that does not require a high-NA objective and is compatible with live cells. Typically, 6-8 W from a 1064-nm laser is required to generate force for cell deflection, and details relevant to the optical design of the trap laser has been discussed in a previous report by Davis et al.[29]

The sorting process is illustrated in Figure 1. First, the flow is biased to direct cells into the waste channel. The trap-laser is focused to a place close to the junction of collection and waste channels and slightly below the sample stream. The trap laser is only turned on (and moves from the lowest position of the triangle along the direction of the arrows shown in Figure 1) after the LabView software makes a

sorting decision, based on the thresholds of the desired photo-physics for the experiment. The LabView software measures the distance between A and B when the pixel positions of lifetime and timing beam are entered. From the transit time of cells from A to B (T_{AB}) and the physical distance between them, the velocity of the cells in the microfluidic channel is computed. From the measured cell velocity and the distance from B to C and C to D, the transit time of the cell to travel BC (T_{BC}) and CD (T_{CD}) are calculated. T_{BC} and T_{CD} determine the delay time and the sweeping velocity of the trap laser so that the trap laser intercepts the cell and deflects it to the collection channel. However, the speed of the cells is not uniform in the microfluidic channel and tends to decrease in the sorting junction. To account for this effect, another adjustable parameter (Extra Delay) was added in the software. The value of the Extra Delay parameter is optimized to increase the sorting efficiency through visual inspection of the cell trajectory in the camera. Once the sorting efficiency is optimized, mutants with improved photo-physical properties can be sorted based on user-defined thresholds.

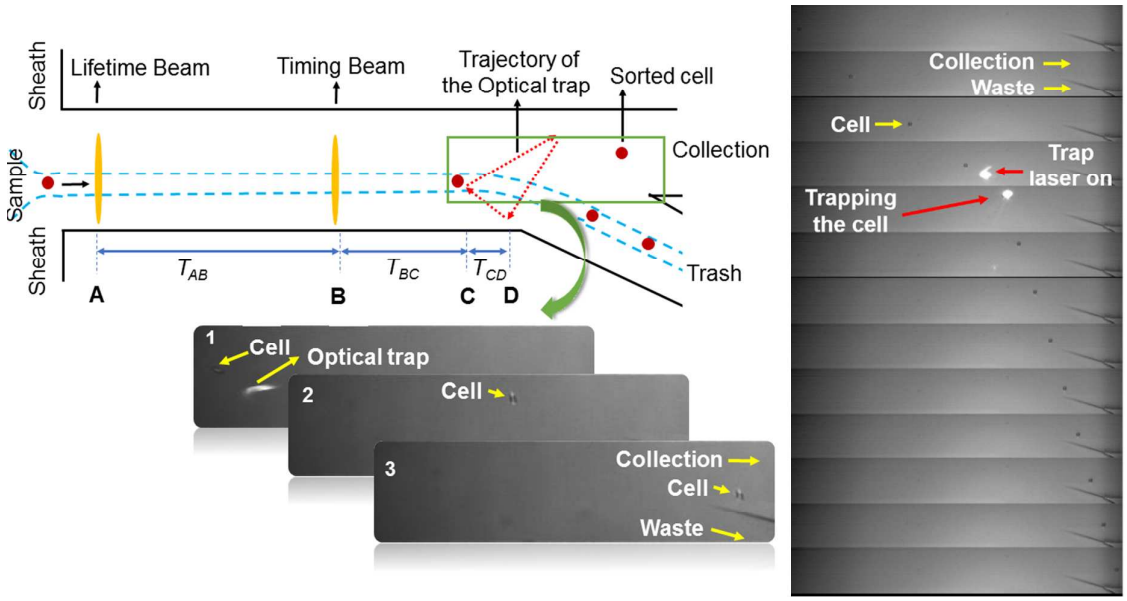

Figure 1: (Left) Sorting of improved RFP variants with optical gradient force switching. The details of the sorting procedure are described in the main text. A portion of the microfluidic is zoomed in to display a yeast cell being sorted into the collection channel. (Right) The stack of images displaying multiple frames of a yeast cell in flow being sorted by the trap laser.

After the enrichment of a subpopulation by microfluidics, the FP library is expressed in agar plates. Next, single mutants are picked from the plates guided by the individual colony lifetimes for further characterizations. The lifetime of an individual colony was measured in a fashion similar to the in-flow phase fluorimetry. The lifetime beam (Figure 1) was manually focused onto single colonies at a low excitation intensity to avoid saturation of the PMT. The PMT signal was demodulated by the lock-in amplifier (Zurich Instruments, UHF). The resulting in-phase and in-quadrature outputs were digitized and processed to extract fluorescence lifetime values. To verify the performance of this technique, mCherry and TagRFP-T colonies were used as references. Each plate contained ~200 colonies and it took ~30 minutes to screen the plate manually based on fluorescence lifetime of

individual colonies. If the FP libraries were plated and screened without microfluidic enrichment for the selection of mutants, it would take ~75 hrs. to screen ~30,000 cells. However, automated cell/colony-picking can enhance the speed of plate-based selections[35].

RESULTS

Error-prone FusionRed Library

We first generated a random mutagenesis library (EP-PCR library) then subjected it to multiple rounds of multi-parametric microfluidic sorting to select the desired sub-library, followed by plating and selection of colonies based on excited state lifetime. Figure 2 displays the screening results of FusionRed (wild-type) and the EP-PCR library expressed in yeast. The library contained a small population (~ 5 %) with longer excited state lifetime than the wild-type FusionRed. Three rounds of microfluidic sorting were performed to enrich this population (Figure 2b; population in the pink box) with a selection gate: lifetime > 2.2 ns. In each round of sorting, typically ~2500 cells were isolated from a pool of ~30,000 cells and grown thereafter for subsequent sorting. Following these enrichments, the library was expressed on galactose-containing plates. Approximately 20 mutants of FusionRed were selected from these plates, guided by the excited state lifetime of the colonies (Experimental Section).

Out of several FR mutants selected from the lifetime-enriched libraries, the excited state lifetimes of FR-1 and FR-13 were found to be 2.5 ns and 2.8 ns (measured in microfluidic screening) respectively, which was significantly higher than the lifetime of FusionRed (2.0 ns). Though FR-1 has shorter excited state lifetime comparing to

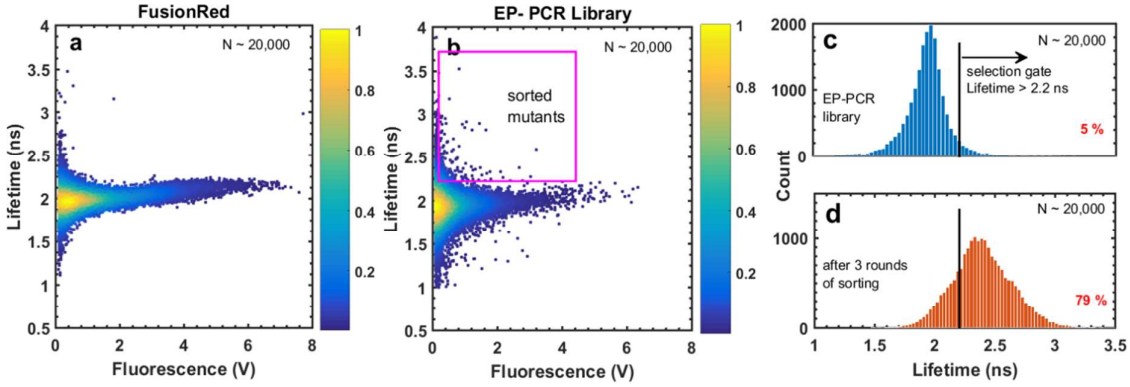

FR-13, its high cellular brightness shows its potential. Therefore, FR-1 and FR-13 were chosen as templates to engineer mutants with higher brightness. Some clones exhibit longer lifetimes but low brightness, this can be either due to reduced extinction coefficients at 561nm excitation or poor expression of such FP mutants at the cellular level. Thus, some clones with longer lifetime and low brightness may be a consequence of heterogeneity in expression levels.

Figure 2: Microfluidic screening dot plots displaying lifetime and brightness (fluorescence signal in volts) profiles of FusionRed (pseudocolor indicates the normalized cell counts at a certain value of brightness and lifetime on the plot – from yellow indicating the highest till indigo indicating lowest) (a) and the FusionRed EP-

PCR library (b) generated by random mutagenesis. The library contained a population with longer lifetime (enclosed in the pink box). (c, d) The EP-PCR library was subjected to microfluidic-based sorting to enrich the population with lifetime longer than 2.2 ns. After three rounds of sorting, the percentage of the population with lifetime longer than 2.2 ns increased from 5% to 79%. The FR-13 and FR-1 mutants were selected from this lifetime-enriched population.

FR-13 Mutant

FR-13 was expressed and purified from *E. coli* and a series of photo-physical characterizations were carried out. Table 1 displays the photo-physical properties of FR-13 and FusionRed. As expected, measurements in purified protein revealed a significant increase in lifetime of FR-13 compared to FusionRed. The ~1.5-fold increase in lifetime of FR-13 correlated with an approximate ~1.8-fold enhancement in quantum yield as compared to its precursor, FusionRed. The *in vitro* brightness calculated from the values of ε_{max} and φ of this mutant is ~2.6 fold higher than FusionRed wild-type. The *in vitro* brightness of FR-13 reflects the effectiveness of selection based on the correlation between excited state lifetime and quantum yield in the perspective of photo-physics. However, the brightness of FR-13 measured by FACS screening (Table 1) and microfluidic screening (Figure 3c) in yeast showed that it was dimmer than FusionRed. These inconsistencies between *in vivo* and *in vitro* brightness of FR-13 may be attributed to its slower chromophore maturation or lower expression efficiency in yeast.

Sequencing of FR-13 revealed the following mutations relative to FusionRed: H25Y, V49I, F83Y and A224T. The amino acid residues were numbered by aligning the sequence of the FR mutants with the avGFP sequence as done in the original report on FusionRed[9]. The sequence alignment is presented in SI-Sec. 10.

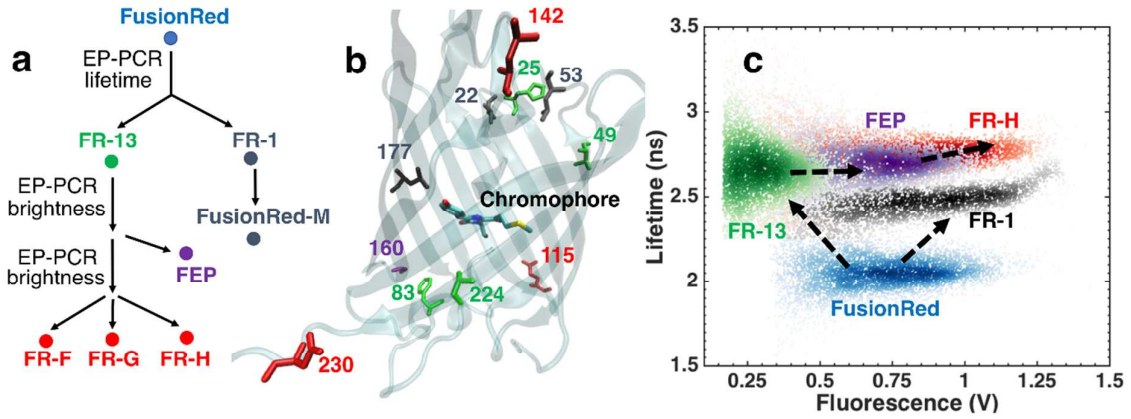

Figure 3: **Directed Evolution of FusionRed**: (a) Genealogy of the FusionRed mutants. FR-13 was generated from the error-prone mutagenesis library of FusionRed and subsequent selection based on excited state lifetime of the mutants. Two rounds of random mutagenesis on FR-13 and selection based on brightness

405 produced FR-F, FR-G and FR-H mutants with improved brightness upon yeast
406 expression, whereas one round gave the FEP mutant. In a separate evolutionary
407 route, FusionRed-M was generated from FR-1 which showed ~2-fold higher
408 brightness than FusionRed in mammalian cell line. (b) Mutations introduced at the
409 first (green), second (purple) and third rounds (red) of EP-PCR mutagenesis during
410 the evolution of FR-13 and FR-13 mutants. Amino acid residues involved in FR-1
411 mutant are displayed in black. Location of the amino acid residues are shown in the
412 crystal structure of mKate (PDB: 3bxb). VMD[40] was used to generate this structure.
413 (c) Evolution trajectory of the FusionRed mutants displaying their lifetime and
414 brightness (fluorescence signal in volts) profiles. Individual mutants were expressed
415 in yeast and screened in the microfluidic platform with ~5000 cells. The screening
416 results were overlaid with different color maps to generate this plot.

417

418 To improve the *in vivo* brightness of FR-13, we first investigated the roles of the four
419 mutations. Of these, only position 224 was internal (facing into the β-barrel) while
420 others were located either in the α–helix (F83) or facing outward of the barrel (H25 &
421 V49). We reverted the mutations individually back to the original FusionRed residues
422 (i.e. constructed FR-13 Y25H, FR-13 I49V, FR-13 Y83F and FR-13 T224A) and
423 performed microfluidic screening in yeast cells. We observed that introduction of a
424 T224A mutation in FR-13 resulted in improved brightness and reduced excited state
425 lifetime (SI-Fig. S6), and therefore concluded that the longer lifetime and lower
426 brightness of FR-13 originated solely from the A224T mutation.
427
428 These photo-physical measurements led us to hypothesize that targeting of position
429 224 with full saturated mutagenesis might yield FR-13 mutants with similar or higher
430 lifetime and improved brightness. However, the site-directed libraries generated by
431 targeting only A224 or in combination with other positions mutated in FR-13 *i.e.* H25,
432 V47 & F83 did not produce variants with higher brightness or longer lifetime. We
433 therefore turned to a random mutagenesis approach.
434
435 Multiple rounds of error-prone mutagenesis on FR-13 and subsequent microfluidic
436 enrichment based on brightness generated three mutants (Figure 3 & SI-Fig. S7)
437 that showed improved brightness in yeast: FR-F, FR-G and FR-H. Purification of
438 these mutants and *in vitro* characterization revealed higher molecular brightness
439 (quantum yield x extinction coefficient) relative to FusionRed (Table 1). The details of
440 the evolution of FR-13 mutants is described in SI-Sec. 9.
441
442 FR-F, G and H mutants showed higher brightness in yeast (Figure 4a), thus could be
443 useful for expressing in yeast considering the advantages of FusionRed mutants.
444 However, when they were expressed in mammalian cells, brightness was not
445 significantly higher relative to FusionRed. Sequence analysis showed the presence
446 of a V4M mutation in all of the mutants (SI-Sec. 10). During the evolution of mKate2
447 from mKate, the M4V mutation was introduced to create an optimal Kozak sequence
448 and efficient expression in the mammalian cells[36]. Another study based on FACS-
449 seq indicated that multiple initiation sites, as observed in these mutants, could be
450 detrimental for the effective expression of the proteins in the mammalian cells[37].
451 From these analyses, we hypothesized that reversing the V4M mutations in these
452 mutants could improve their expression efficiency and brightness in mammalian
453 cells. Hence, we generated the FRX mutants: XF (FR-F, M4V); XG (FR-G, M4V); XH

(FR-H, M4V). However, when stably expressed in MCF10A cell-line, the brightness of these FRX mutants was lower than FusionRed. This inconsistency in brightness of the FRX mutants is most likely due to lower expression efficiency or slower chromophore maturation in mammalian cells. As multiple attempts to improve the brightness of FR-13 in mammalian cell line were unsuccessful, we focused on the FR-1 mutant

Table 1: Photo-physical properties of the mutants derived from FR-13. Brightness values in yeast are the mean fluorescence intensity in the cells expressing the mutants as measured by FACS (Figure 4a). Values of λ_{abs} and λ_{em} are the maximum wavelengths of visible absorption and emission spectra, respectively, τ is the excited state lifetime, φ is the fluorescence quantum yield, and ε_{max} is the extinction coefficient at the absorption peak. Details of photo-physical measurements are described in SI-Sec. 11.

RFP	λ_{abs} (nm)	λ_{em} (nm)	τ (ns)	φ	ε_{max} (M^{-1} cm^{-1})	Molecular Brightness (ε×φ)	Brightness (in yeast)
FusionRed	575	596	1.8	0.26	87,300	100	100
FR-13	571	591	2.7	0.48	124,000	262	27
FR-F	571	591	2.6	0.36	104,000	165	138
FR-G	572	591	2.7	0.42	105,000	194	144
FR-H	572	592	2.6	0.42	90,100	167	142

FR-1 Mutant

FR-1 was found to have a longer lifetime and higher quantum yield compared to FusionRed (Table 2). Although the *in vitro* brightness of FR-1 was found to be only 30% higher than FusionRed, when expressed in yeast it showed ~3.5-fold higher brightness (SI-Sec. 12).

The FR-1 mutant has the following mutations relative to FusionRed: V22I, L53P and L177M. The L177 sidechain points into the β-barrel and is located close to the chromophore. On the other hand, L53 and V22 are located in the loop region (Figure 3b). From our previous experience with FR-13 mutants, we hypothesized that due to its proximity to the chromophore, L177 may be crucial in modifying the photo-physical properties in FR-1. We therefore generated FusionRed L177M (named as FusionRed-M and abbreviated as FR-M). Table 2 compares the photo-physical properties of FusionRed, FR-1 and FusionRed-M. Both FR-1 and FusionRed-M mutants have higher *in vitro* brightness relative to FusionRed. However, FusionRed-M performs better than FR-1 when transiently expressed in the nuclei of the HeLa cells (H2B-RFP construct). Quantification of brightness in HeLa cells with three biological replicates reveals that FusionRed-M is ~2-fold brighter than FusionRed

and has similar brightness as mCherry (Figure 4b), which is the most widely used RFP.

Table 2: Photo-physical properties of the mutants derived from FR-1. Brightness in mammalian (HeLa) cells presented here are the mean fluorescence intensity of the cells expressing the mutants as measured in FACS screening (Figure 4b). λ_{abs} and λ_{em} are the maximum wavelengths of visible absorption and emission spectra, respectively. τ is the excited state lifetime. φ is the fluorescence quantum yield. ε_{max} is the extinction coefficient at the absorption peak. Details of photo-physical characterization are described in SI-Sec. 11.

RFP	λ_{abs} (nm)	λ_{em} (nm)	τ (ns)	φ	ε_{max} ($M^{-1}cm^{-1}$)	Molecular Brightness (ε×φ)	Brightness (in HeLa)
FusionRed	575	596	1.8	0.26	87,300	100	100
FR-1	569	594	2.3	0.34	84,900	127	116
FusionRed-M	571	594	2.1	0.34	71,100	107	191

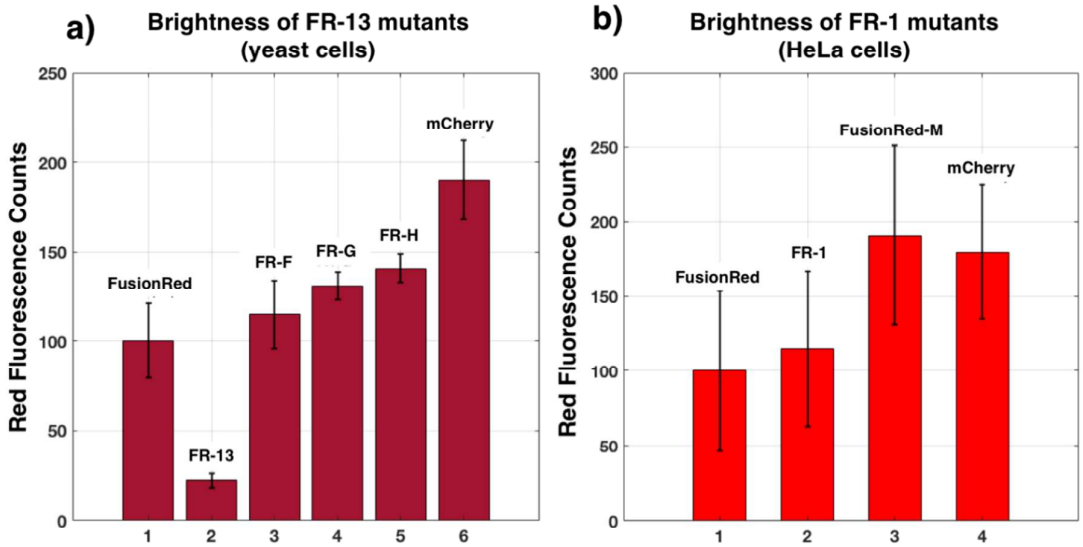

Figure 4: Mean red fluorescence intensities averaged from three biological replicates relative to FusionRed. (a) 20,000 cells were FACS screened after ~18 hrs. post-induction in the cytoplasm of yeast cells for each RFP. (b) 10,000 cells were FACS screened after ~48 hrs. post-transfection in HeLa cell-lines (H2B-RFP constructs) for each RFP. Details are described in SI-Sec. 12. FusionRed-M displayed ~2-fold higher brightness relative to its precursor FusionRed in the HeLa cell line, and FR-F, G, and H clones showed higher brightness in yeast cells compared to the precursor FR-13.

OSER Assay

Directed evolution of FusionRed generated multiple mutants that showed higher brightness in yeast (FR-F, FR-G, FR-H, FR-1) and mammalian cell lines (FR-1, FusionRed-M). Next, we investigated whether the additional mutations in FusionRed introduced any detrimental effect on its monomeric character. The *in vivo* dimerization tendency of FusionRed mutants were carried out by performing the organized smooth endoplasmic reticulum (OSER) assay[38]. FPs were fused to the cytoplasmic-end of endoplasmic reticulum (ER) signal anchor membrane protein (CytERM) and expressed in HeLa cells. FPs with *in vivo* oligomeric tendencies tend to interact with each other, driving the restructuring of the reticular architecture of ER. This leads to the formation of OSER, which is manifested by small, bright puncta or whorls in fluorescence imaging (Figure 5b). The OSER score, defined as the percentage of cells expressing CytERM-RFP constructs displaying no whorl, can be used to quantify the *in vivo* dimerization tendency, i.e. an OSER score of 100 or 0 refers to a completely monomeric or oligomeric FP, respectively.

The identification of whorls from a large number of cells is required to obtain a statistically robust OSER score. This process is tedious and subject to human bias and errors. To account for these issues, we developed a custom-based image analysis program based on CellProfiler[39]. Detailed description of sample preparation, image acquisition and analysis with this program are given in SI-Sec. 14 and SI-Sec. 15.

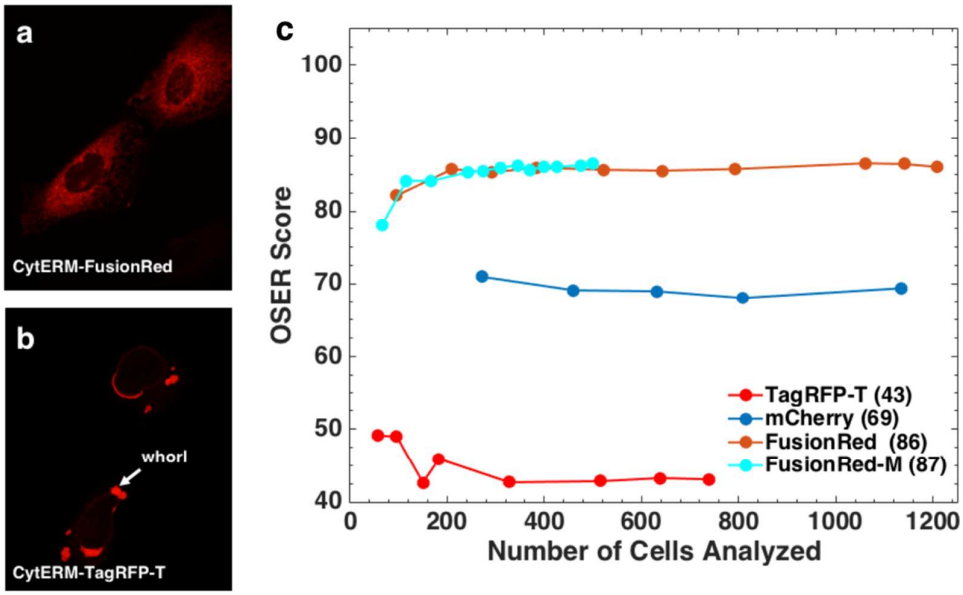

Figure 5: **OSER assay of the FusionRed mutants**: (a, b) U2OS cells expressing CytERM-FusionRed and CytERM-TagRFP-T constructs. Most of the cells expressing CytERM-FusionRed constructs displayed proper localization with reticular-like structures while TagRFP-T, owing to its in vivo oligomerization tendencies, showed small (1-7 μm), bright puncta (whorls), upon fusion to CytERM. (c) OSER score of RFPs.

Figure 5c displays the OSER score of various RFPs as a function of number of cells analyzed. It is evident that analysis of ~300 cells is sufficient to obtain a stable OSER score. Different parameters and thresholds of the image analysis program were adjusted with the known OSER score of TagRFP-T (positive control) and FusionRed (negative control)[32]. As shown in Figure 5c, TagRFP-T and FusionRed showed an OSER score of 43 and 86 respectively, which is close to the value obtained by Cranfill et al. by analyzing 10,000 cells for each FP (41.2 and 91.5 for TagRFP-T and FusionRed respectively)[32]. In our hands, mCherry showed a low OSER score, in contrast with previous reports[16, 32]. FusionRed and FusionRed-M mutants showed high OSER scores indicating low *in vivo* oligomerization tendencies. This suggests that the increased brightness of FusionRed-M and other FusionRed mutants did not compromise the monomeric character of FusionRed under physiological conditions.

DISCUSSION

A microfluidic sorter capable of selecting members of cell-based FP libraries based on their excited state lifetime and fluorescence intensity has been used for the directed evolution of brightness in FusionRed. The selected mutants expressed in yeast show an improvement in lifetime and fluorescence quantum yield, resulting in higher brightness (Figure 4a). FusionRed-M developed from the FR-1 mutant displayed ~2-fold increase in brightness upon transient expression (H2B-RFP construct) in HeLa cells (Figure 4b). Although the molecular brightness of an FP only depends on its extinction coefficient and fluorescence quantum yield, the practical brightness in cells is a function of additional biochemical factors. For example, it depends on chromophore maturation, expression efficiency and chemical environment of the cellular compartment[41].

FR-13 shows improved *in vitro* brightness relative to its precursor (FusionRed) due to its enhanced ε_{max} and ϕ. However, upon expression in yeast, FR-13 showed lower brightness. Further rounds of mutagenesis were required to improve its brightness in yeast. This result indicates that selection based on molecular photo-physical parameters such as fluorescence lifetime indeed provides the desirable improvement in molecular brightness, but it does not guarantee the brightness in cells.

Figure 3b displays the mutations involved in the course of evolving FusionRed. The first round of mutagenesis generated FR-13 and FR-1 mutants. FR-13 contains mutations at positions 25, 49, 83 and 224 (Figure 3b, shown in green). Photo-physical analysis of the individual FR-13 point mutants revealed that the A224T modification is responsible for its improved lifetime and quantum yield as well as its reduced *in vivo* brightness. The first and second rounds of mutagenesis on FR-13 introduced the modifications at position 160 (shown in purple) and positions 4, 115, 142 and 230 (shown in red), which progressively improved the brightness in yeast without affecting the lifetime. These positions are located either in loop regions or pointing out of the β-barrel. Initially, we hypothesized that mutations at these amino acid residues increase maturation speed or enhance expression efficiency and thereby increasing *in vivo* brightness of FR-13. However, these variants were found to have similar maturation kinetics as FR-13 in yeast (SI-Fig. S9). Therefore, we attribute the low brightness of FR-13 in yeast to its lower expression efficiency as estimated and compared with FusionRed and mCherry in SI-Sec. 13. We suggest

that further mutations in FR-13 have alleviated this limitation and generated FR-F, FR-G and FR-H mutants with higher brightness in yeast.

On the other hand, FR-1 mutant displayed significant improvement upon expression in yeast. It was shown that L177M mutation was responsible for the improved lifetime and quantum yield of FR-1. Introduction of L177M mutation in wild-type FusionRed generated FusionRed-M mutant which displays ~2-fold higher brightness than its precursor FusionRed when expressed in mammalian cell line. Despite the improvement in lifetime and quantum yield, FusionRed-M exhibited a reduced extinction coefficient relative to FusionRed, leading to a limited increase in molecular brightness. Therefore we attribute the enhanced brightness of FusionRed-M in mammalian cells to improved protein expression level. As estimated in SI-Sec. 13, the expression level of FusionRed-M is nearly 2 fold greater than FusionRed and 70% of mCherry. The improved expression level (relative to FusionRed) and higher fluorescence quantum yield (relative to mCherry) result in the brightness of FusionRed-M comparable with mCherry when expressed in mammalian cells. Though FusionRed-M was obtained by reverse engineering based on findings from FR-1, this result suggests that if the selection was performed only based on the brightness of FACS screening, it could lead to improved brightness in cells but not necessarily in the molecular level (i.e. molecular brightness).

The OSER assay demonstrated the highly monomeric character of FusionRed-M compared to mCherry, the most widely used RFP. Depending on the biological application of RFP tools, when the monomeric character of RFPs becomes a crucial criterion, FusionRed-M aym be a good substitution for mCherry or other RFPs with less or poor monomeric character.

Brightness is not the only photo-physical property of importance in fluorescence imaging. The ability to select on complex criteria such as photostability, chromophore maturation and photoswitching will play an important role in the development of new FPs. We previously demonstrated that measurement of photostability can also be implemented in a microfluidic sorter, enabling the selection of FP mutants with reduced photobleaching, though at the expense of reduced fluorescence lifetime and brightness.[31] In the current sorting system, an additional blue excitation laser can also be incorporated to monitor the completeness of chromophore formation and thereby eliminate immature RFP mutants with green emission[42]. We also reported a frequency-domain approach for quantifying dark-state conversion (DSC) kinetics in FPs[43]. This technique can also be employed in a flow system for selections to generate photostable or photo-switchable FPs. When incorporated with multiple photo-physical parameters, we expect that this microfluidic system could be used to gain a better and more comprehensive understanding of the fitness landscape of FPs. This is essential for the overall development of FPs for broader utility in imaging applications.

CONCLUSIONS

We have presented a microfluidic sorter that can be utilized to select mutants from fluorescent protein libraries based on their excited state lifetime and fluorescence intensity, and visualize of the trajectory of FP evolution. We demonstrated its ability by engineering variants of the FusionRed RFP with improved photo-physical

properties. With multiple rounds of error-prone mutagenesis and sorting based on fluorescence lifetime and intensity, a set of mutants is generated with a significant improvement in lifetime. This enhancement in lifetime results in an increase in fluorescence quantum yield and more than 2-fold improvement in theoretical brightness (extinction coefficient x quantum yield) of the FPs. The mutants displayed significantly higher brightness in yeast relative to their precursor. A single mutation (L177M) in FusionRed enhanced its brightness by ~2-fold as evidenced by mammalian cell expression. Quantification of *in vivo* dimerization propensity of the mutants indicates that the improvement in brightness is achieved without sacrificing the monomeric character of FusionRed. At different phases of the evolution process, mutants are isolated and their photo-physical/bio-chemical properties are quantified. This enables us to visualize the trajectory of directed evolution in FusionRed. Mutations associated with error-prone mutagenesis have been discussed in the context of their role in modifying lifetime, maturation speed and expression efficiency. These investigations revealed that directed evolution on fluorescence lifetime is capable of achieving improvements in brightness within a specific host organism. Fortunately, microfluidic sorting is compatible with a wide range of cells and organisms such as bacteria, yeast, mammalian and plant cells. Furthermore, the microfluidic sorter can be modified to incorporate other photo-physical parameters, e.g. photostability, dark state conversion etc. This will be useful for simultaneous improvement and monitoring of multiple essential photo-physical properties of FPs and has the potential for a more comprehensive understanding of their fitness landscapes.

CONFLICTS OF INTEREST

There are no conflicts of interest to declare.

ASSOCIATED CONTENT

Supplementary Information of this article contains the details of microfluidic design and manifold assembly, schematic of electronics and signal processing, comparative screening results with linear and logarithmic amplifier, theory of frequency-domain lifetime measurements in flow cytometry, characterization of the single mutants of FR-13 and sequence alignment of the FusionRed mutants etc.

ACKNOWLEDGEMENTS

This work was supported by the NSF Physics Frontier Center at JILA (PHY 1734006 to R.J.) and NIH DP1 GM114863 and R01 GM084027 (to A.E.P). RJ is a staff member in the Quantum Physics Division of the National Institute of Standards and Technology (NIST). Certain commercial equipment, instruments, or materials are identified in this paper in order to specify the experimental procedure adequately. Such identification is not intended to imply recommendation or endorsement by the NIST, nor is it intended to imply that the materials or equipment identified are necessarily the best available for the purpose. We acknowledge the Flow Cytometry facility at BioFrontiers Institute, CU Boulder (grant # S10ODO21601). The imaging work was performed at the BioFrontiers Institute Advanced Light Microscopy Core. Spinning disc confocal microscopy was performed on Nikon Ti-E microscope supported by the BioFrontiers Institute and the Howard Hughes Medical Institute. We

thank Dr. Joe Dragavon for helpful discussion on confocal imaging. Fluorescence measurements were performed at Biochemistry Shared Instruments Pool. The absorption measurement was performed at JILA Keck Laboratory. Structure figures were made with VMD, which was developed by the Theoretical and Computational Biophysics Group in the Beckman Institute for Advanced Science and Technology at the University of Illinois at Urbana-Champaign.

REFERENCES

1. E. A. Rodriguez, R. E. Campbell, J. Y. Lin, M. Z. Lin, A. Miyawaki, A. E. Palmer, X. K. Shu, J. Zhang and R. Y. Tsien, *Trends Biochem Sci*, 2017, **42**, 111-129.
2. S. Waldchen, J. Lehmann, T. Klein, S. van de Linde and M. Sauer, *Sci Rep*, 2015, **5**, 15348(1-12).
3. E. A. Rodriguez, G. N. Tran, L. A. Gross, J. L. Crisp, X. K. Shu, J. Y. Lin and R. Y. Tsien, *Nat Methods*, 2016, **13**, 763-769.
4. G. Matela, P. Gao, G. Guigas, A. F. Eckert, K. Nienhaus and G. U. Nienhaus, *Chem Commun (Camb)*, 2017, **53**, 979-982.
5. K. D. Piatkevich, V. N. Malashkevich, K. S. Morozova, N. A. Nemkovich, S. C. Almo and V. V. Verkhusha, *Scientific Reports*, 2013, **3**, 1847(1-11).
6. J. Chu, R. D. Haynes, S. Y. Corbel, P. P. Li, E. Gonzalez-Gonzalez, J. S. Burg, N. J. Ataie, A. J. Lam, P. J. Cranfill, M. A. Baird, M. W. Davidson, H. L. Ng, K. C. Garcia, C. H. Contag, K. Shen, H. M. Blau and M. Z. Lin, *Nat Methods*, 2014, **11**, 572-578.
7. N. C. Shaner, R. E. Campbell, P. A. Steinbach, B. N. G. Giepmans, A. E. Palmer and R. Y. Tsien, *Nature Biotechnology*, 2004, **22**, 1567-1572.
8. N. C. Shaner, M. Z. Lin, M. R. McKeown, P. A. Steinbach, K. L. Hazelwood, M. W. Davidson and R. Y. Tsien, *Nat Methods*, 2008, **5**, 545-551.
9. I. I. Shemiakina, G. V. Ermakova, P. J. Cranfill, M. A. Baird, R. A. Evans, E. A. Souslova, D. B. Staroverov, A. Y. Gorokhovatsky, E. V. Putintseva, T. V. Gorodnicheva, T. V. Chepurnykh, L. Strukova, S. Lukyanov, A. G. Zaraisky, M. W. Davidson, D. M. Chudakov and D. Shcherbo, *Nat Commun*, 2012, **3**, 1204(1-7).
10. Y.-T. Kao, X. Zhu and W. Min, *P Natl Acad Sci USA*, 2012, **109**, 3220-3225.
11. J. Goedhart, D. von Stetten, M. Noirclerc-Savoye, M. Lelimousin, L. Joosen, M. A. Hink, L. van Weeren, T. W. J. Gadella and A. Royant, *Nat Commun*, 2012, **3**, 751(1-9).
12. E. M. Merzlyak, J. Goedhart, D. Shcherbo, M. E. Bulina, A. S. Shcheglov, A. F. Fradkov, A. Gaintzeva, K. A. Lukyanov, S. Lukyanov, T. W. J. Gadella and D. M. Chudakov, *Nat Methods*, 2007, **4**, 555-557.
13. H. Mizuno, P. Dedecker, R. Ando, T. Fukano, J. Hofkens and A. Miyawaki, *Photochemical & Photobiological Sciences*, 2010, **9**, 239-248.
14. S. Duwe, E. De Zitter, V. Gielen, B. Moeyaert, W. Vandenberg, T. Grotjohann, K. Clays, S. Jakobs, L. Van Meervelt and P. Dedecker, *Acs Nano*, 2015, **9**, 9528-9541.
15. J. Goedhart, L. van Weeren, M. A. Hink, N. O. E. Vischer, K. Jalink and T. W. J. Gadella, *Nat Methods*, 2010, **7**, 137-139.

16. D. S. Bindels, L. Haarbosch, L. van Weeren, M. Postma, K. E. Wieser, M. Mastop, S. Aumonier, G. Gotthard, A. Royant, M. A. Hink and T. W. J. Gadella, *Nat Methods*, 2017, **14**, 53-56.
17. K. P. Carter, M. C. Carpenter, B. Fiedler, R. Jimenez and A. E. Palmer, *Anal Chem*, 2017, **89**, 9601-9608.
18. N. B. Arnfinnsdottir, A. V. Bjorkoy, R. Lale and M. Sletmoen, *Rsc Adv*, 2016, **6**, 36198-36206.
19. L. Wang, W. C. Jackson, P. A. Steinbach and R. Y. Tsien, *P Natl Acad Sci USA*, 2004, **101**, 16745-16749.
20. J. Nedbal, V. Visitkul, E. Ortiz-Zapater, G. Weitsman, P. Chana, D. R. Matthews, T. Ng and S. M. Ameer-Beg, *Cytom Part A*, 2015, **87a**, 104-118.
21. B. G. Pinsky, J. J. Ladasky, J. R. Lakowicz, K. Berndt and R. A. Hoffman, *Cytometry*, 1993, **14**, 123-135.
22. J. A. Steinkamp and H. A. Crissman, *Cytometry*, 1993, **14**, 210-216.
23. C. Deka, B. E. Lehnert, N. M. Lehnert, G. M. Jones, L. A. Sklar and J. A. Steinkamp, *Cytometry*, 1996, **25**, 271-279.
24. H. H. Cui, J. G. Valdez, J. A. Steinkamp and H. A. Crissman, *Cytom Part A*, 2003, **52a**, 46-55.
25. R. Cao, V. Pankayatselvan and J. P. Houston, *Opt Express*, 2013, **21**, 14816-14831.
26. J. P. Houston, M. A. Naivar and J. P. Freyer, *Cytom Part A*, 2010, **77a**, 861-872.
27. B. Sands, P. Jenkins, W. J. Peria, M. Naivar, J. P. Houston and R. Brent, *Plos One*, 2014, **9**, e109940(1-11).
28. Z. H. Yang, D. M. Shcherbakova, V. V. Verkhusha and J. P. Houston, *2016 Conference on Lasers and Electro-Optics (Cleo)*, 2016,(1-3).
29. L. M. Davis, J. L. Lubbeck, K. M. Dean, A. E. Palmer and R. Jimenez, *Lab Chip*, 2013, **13**, 2320-2327.
30. K. M. Dean, J. L. Lubbeck, L. M. Davis, C. K. Regmi, P. P. Chapagain, B. S. Gerstman, R. Jimenez and A. E. Palmer, *Integrative Biology*, 2015, **7**, 263-273.
31. K. M. Dean, L. M. Davis, J. L. Lubbeck, P. Manna, P. Friis, A. E. Palmer and R. Jimenez, *Anal Chem*, 2015, **87**, 5026-5030.
32. P. J. Cranfill, B. R. Sell, M. A. Baird, J. R. Allen, Z. Lavagnino, H. M. de Gruiter, G. J. Kremers, M. W. Davidson, A. Ustione and D. W. Piston, *Nat Methods*, 2016, **13**, 557-562.
33. J. L. Lubbeck, K. M. Dean, H. Ma, A. E. Palmer and R. Jimenez, *Anal Chem*, 2012, **84**, 3929-3937.
34. W. M. Patrick, A. E. Firth and J. M. Blackburn, *Protein Eng*, 2003, **16**, 451-457.
35. K. D. Piatkevich, E. E. Jung, C. Straub, C. Y. Linghu, D. Park, H. J. Suk, D. R. Hochbaum, D. Goodwin, E. Pnevmatikakis, N. Pak, T. Kawashima, C. T. Yang, J. L. Rhoades, O. Shemesh, S. Asano, Y. G. Yoon, L. Freifeld, J. L. Saulnier, C. Riegler, F. Engert, T. Hughes, M. Drobizhev, B. Szabo, M. B. Ahrens, S. W. Flavell, B. L. Sabatini and E. S. Boyden, *Nat Chem Biol*, 2018, **14**, 352-360.
36. D. Shcherbo, C. S. Murphy, G. V. Ermakova, E. A. Solovieva, T. V. Chepurnykh, A. S. Shcheglov, V. V. Verkhusha, V. Z. Pletnev, K. L. Hazelwood, P. M. Roche, S. Lukyanov, A. G. Zaraisky, M. W. Davidson and D. M. Chudakov, *Biochemical Journal*, 2009, **418**, 567-574.

37. W. L. Noderer, R. J. Flockhart, A. Bhaduri, A. J. D. de Arce, J. J. Zhang, P. A. Khavari and C. L. Wang, *Mol Syst Biol*, August 2014, **10**, 748(1-14).
38. L. M. Costantini, M. Fossati, M. Francolini and E. L. Snapp, *Traffic*, 2012, **13**, 643-649.
39. L. Kamentsky, T. R. Jones, A. Fraser, M. A. Bray, D. J. Logan, K. L. Madden, V. Ljosa, C. Rueden, K. W. Eliceiri and A. E. Carpenter, *Bioinformatics*, 2011, **27**, 1179-1180.
40. W. Humphrey, A. Dalke and K. Schulten, *J Mol Graph Model*, 1996, **14**, 33-38.
41. E. Balleza, J. M. Kim and P. Cluzel, *Nat Methods*, 2018, **15**, 47-51.
42. K. B. Bravaya, O. M. Subach, N. Korovina, V. V. Verkhusha and A. I. Krylov, *J Am Chem Soc*, 2012, **134**, 2807-2814.
43. P. Manna and R. Jimenez, *Journal of Physical Chemistry B*, 2015, **119**, 4944-4954.

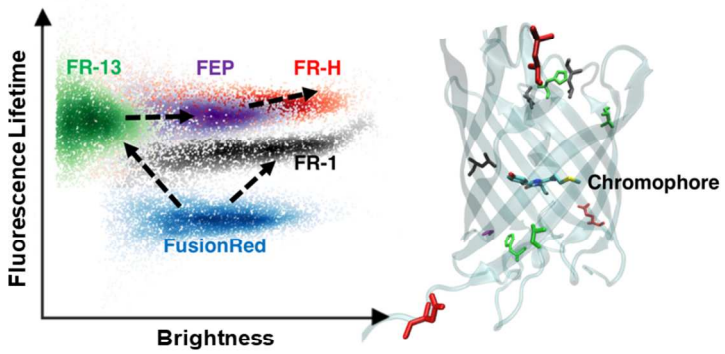

Directed evolution of fluorescent proteins with lifetime and brightness selections leads to improved variants.